Transition from thermal diffusion to heat accumulation in high repetition rate femtosecond laser writing of buried optical waveguides

Shane M. Eaton, Haibin Zhang, Mi Li Ng, Jianzhao Li, Wei-Jen Chen, Stephen Ho and Peter R. Herman

Edward S. Rogers Department of Electrical and Computer Engineering and Institute for Optical Sciences
University of Toronto, 10 King's College Road, Toronto, ON M5S-3G4 Canada
shane.eaton@utoronto.ca

Abstract: A variable (0.2 to 5 MHz) repetition rate femtosecond laser was applied to delineate the role of thermal diffusion and heat accumulation effects in forming low-loss optical waveguides in borosilicate glass across a broad range of laser exposure conditions. For the first time, a smooth transition from diffusion-only transport at 200-kHz repetition rate to strong heat accumulation effects at 0.5 to 2 MHz was observed and shown to drive significant variations in waveguide morphology, with rapidly increasing waveguide diameter that accurately followed a simple thermal diffusion model over all exposure variables tested. Amongst these strong thermal trends, a common exposure window of 200-mW average power and ~15-mm/s scan speed was discovered across the range of 200-kHz to 2-MHz repetition rates for minimizing insertion loss despite a 10-fold drop in laser pulse energy. Waveguide morphology and thermal modeling indicate that strong thermal diffusion effects at 200 kHz give way to a weak heat accumulation effect at ~1-μJ pulse energy for generating low loss waveguides, while stronger heat accumulation effects above 1-MHz repetition rate offered overall superior guiding. A comprehensive characterization of waveguide properties is presented for laser writing in the thermal diffusion and heat accumulation regimes. The waveguides are shown to be thermally stable up to 800°C and can be written in a convenient 520-μm depth range with low spherical aberration.

OCIS codes: (230.7370) Waveguides; (350.3390) Laser materials processing; (320.2250) Femtosecond phenomena; (160.2750) Glass and other amorphous materials

References and links

1. C. B. Schaffer, J. F. Garcia, and E. Mazur, "Bulk heating of transparent materials using a high-repetition-rate femtosecond laser," Appl. Phys. A **76**, 351-354 (2003).
2. K. Minoshima, A. M. Kowalevicz, I. Hartl, E. P. Ippen, and J. G. Fujimoto, "Photonic device fabrication in glass by use of nonlinear materials processing with a femtosecond laser oscillator," Opt. Lett. **26**, 1516-1518 (2001).
3. R. Osellame, N. Chiodo, G. Della Valle, G. Cerullo, R. Ramponi, P. Laporta, A. Killi, U. Morgner, and O. Svelto, "Waveguide lasers in the C-band fabricated by laser inscription with a compact femtosecond oscillator," IEEE J. Sel. Top. Quantum Electron. **12**, 277-285 (2006).
4. S. M. Eaton, H. Zhang, P. R. Herman, F. Yoshino, L. Shah, J. Bovatsek, and A. Y. Arai, "Heat accumulation effects in femtosecond laser-written waveguides with variable repetition rate," Opt. Express **13**, 4708-4716 (2005).
5. R. Osellame, N. Chiodo, G. D. Valle, S. Taccheo, R. Ramponi, G. Cerullo, A. Killi, U. Morgner, M. Lederer, and D. Kopf, "Optical waveguide writing with a diode-pumped femtosecond oscillator," Opt. Lett. **29**, 1900-1902 (2004).
6. K. M. Davis, K. Miura, N. Sugimoto, and K. Hirao, "Writing waveguides in glass with a femtosecond laser," Opt. Lett. **21**, 1729-1731 (1996).
7. P. R. Herman, A. Oettl, K. P. Chen, and R. S. Marjoribanks, "Laser micromachining of transparent fused silica with 1-ps pulses and pulse trains," Proc. SPIE **3616**, 148-155 (1999).

#95835 - $15.00 USD Received 6 May 2008; revised 5 Jun 2008; accepted 8 Jun 2008; published 11 Jun 2008

8. A. H. Nejadmalayeri, and P. R. Herman, "Rapid thermal annealing in high repetition rate ultrafast laser waveguidewriting in lithium niobate," Opt. Express **15**, 10842-10854 (2007).
9. C. Hnatovsky, R. S. Taylor, E. Simova, V. R. Bhardwaj, D. M. Rayner, and P. B. Corkum, "High-resolution study of photoinduced modification in fused silica produced by a tightly focused femtosecond laser beam in the presence of aberrations," J. Appl. Phys. **98**, 013517 (2005).
10. Corning, "Corning EAGLE2000 AMLCD glass substrates material information," http://www.corning.com/displaytechnologies.
11. C. W. Carr, H. B. Radousky, A. M. Rubenchik, M. D. Feit, and S. G. Demos, "Localized Dynamics during Laser-Induced Damage in Optical Materials," Phys. Rev. Lett. **92**, 087401 (2004).
12. M. Sakakura, M. Terazima, Y. Shimotsuma, K. Miura, and K. Hirao, "Heating and rapid cooling of bulk glass after photoexcitation by a focused femtosecond laser pulse," Opt. Express **15**, 16800-16807 (2007).
13. I. Miyamoto, A. Horn, J. Gottmann, D. Wortmann, and F. Yoshino, "Fusion welding of glass using femtosecond laser pulses with high-repetition rates," J. Laser Micro/Nanoeng. **2**, 57-63 (2007).
14. B. C. Stuart, M. D. Feit, S. Herman, A. M. Rubenchik, B. W. Shore, and M. D. Perry, "Nanosecond-to-femtosecond laser-induced breakdown in dielectrics," Phys. Rev. B **53**, 1749 (1996).
15. J. Li, P. R. Herman, S. M. Eaton, H. Zhang, A. H. Nejadmalayeri, and S. A. Hosseini, "Combining 5-D Microscopy with 3-D Femtosecond Laser Nanoprocessing," in *Conference on Lasers and Electro-Optics* (Optical Society of America, 2007), Talk CFr4.
16. P. Oberson, B. Gisin, B. Huttner, and N. Gisin, "Refracted near-field measurements of refractive index and geometry of silica-on-silicon integrated optical waveguides," Appl. Opt. **37**, 7268-7272 (1998).
17. S. Nolte, M. Will, J. Burghoff, and A. Tünnermann, "Ultrafast laser processing: new options for three-dimensional photonic structures," J. Mod. Opt. **51**, 2533-2542 (2004).
18. J. W. Chan, T. R. Huser, S. H. Risbud, J. S. Hayden, and D. M. Krol, "Waveguide fabrication in phosphate glasses using femtosecond laser pulses," Appl. Phys. Lett. **82**, 2371-2373 (2003).
19. C. B. Schaffer, A. Brodeur, and E. Mazur, "Laser-induced breakdown and damage in bulk transparent materials induced by tightly focused femtosecond laser pulses," Meas. Sci. Technol. **12**, 1784-1794 (2001).
20. H. Zhang, S. M. Eaton, J. Li, A. H. Nejadmalayeri, and P. R. Herman, "Type II high-strength Bragg grating waveguides photowritten with ultrashort laser pulses," Opt. Express **15**, 4182-4191 (2007).
21. R. Gattass, "Femtosecond-laser interactions with transparent materials: applications in micromachining and supercontinuum generation," (PhD thesis, Harvard University, Cambridge, 2006).
22. R. Bruckner, "Metastable equilibrium density of hydroxyl-free synthetic vitreous silica," J. Non-Cryst. Solids **5**, 281-285 (1971).
23. E. G. Gamaly, S. Juodkazis, K. Nishimura, H. Misawa, B. Luther-Davies, L. Hallo, P. Nicolai, and V. T. Tikhonchuk, "Laser-matter interaction in the bulk of a transparent solid: Confined microexplosion and void formation," Phys. Rev. B **73**, 214101 (2006).
24. E. N. Glezer, and E. Mazur, "Ultrafast-laser driven micro-explosions in transparent materials," Appl. Phys. Lett. **71**, 882-884 (1997).
25. L. Shah, A. Arai, S. Eaton, and P. Herman, "Waveguide writing in fused silica with a femtosecond fiber laser at 522 nm and 1 MHz repetition rate," Opt. Express **13**, 1999-2006 (2005).
26. S. M. Eaton, H. Zhang, M. L. Ng, S. Ho, and P. R. Herman, "Optimization of repetition rate, pulse duration, and polarization for femtosecond-laser-writing of waveguides in borosilicate and fused silica glasses," in *Conference on Lasers and Electro-Optics Europe* (Optical Society of America, 2007), Talk CE5-5-WED.
27. H. C. Guo, H. B. Jiang, Y. Fang, C. Peng, H. Yang, Y. Li, and Q. H. Gong, "The pulse duration dependence of femtosecond laser induced refractive index modulation in fused silica," J. Opt. A. **6**, 787-790 (2004).
28. T. Fukuda, S. Ishikawa, T. Fujii, K. Sakuma, and H. Hosoya, "Low-loss optical waveguides written by femtosecond laser pulses for three-dimensional photonic devices," Proc. SPIE **5339**, 524-538 (2004).
29. M. Ams, G. D. Marshall, and M. J. Withford, "Study of the influence of femtosecond laser polarisation on direct writing of waveguides," Opt. Express **14**, 13158-13163 (2006).
30. D. Liu, Y. Li, R. An, Y. Dou, H. Yang, and Q. Gong, "Influence of focusing depth on the microfabrication of waveguides inside silica glass by femtosecond laser direct writing," Appl. Phys. A. **84**, 257-260 (2006).
31. V. Diez-Blanco, J. Siegel, A. Ferrer, A. R. de la Cruz, and J. Solis, "Deep subsurface waveguides with circular cross section produced by femtosecond laser writing," Appl. Phys. Lett. **91**, 051104 (2007).
32. L. McCaughan, and E. J. Murphy, "Influence of temperature and initial titanium dimensions on fiber Ti:lithium niobate waveguide insertion loss at 1.3 microns," IEEE J. Quantum Electron. **19**, 131-136 (1983).
33. C. Hnatovsky, R. S. Taylor, P. P. Rajeev, E. Simova, V. R. Bhardwaj, D. M. Rayner, and P. B. Corkum, "Pulse duration dependence of femtosecond-laser-fabricated nanogratings in fused silica," Appl. Phys. Lett. **87,** 014104 (2005).
34. C. Hnatovsky, R. S. Taylor, E. Simova, P. P. Rajeev, D. M. Rayner, V. R. Bhardwaj, and P. B. Corkum, "Fabrication of microchannels in glass using focused femtosecond laser radiation and selective chemical etching," Appl. Phys. A. **84**, 47-61 (2006).
35. D. M. Rayner, A. Naumov, and P. B. Corkum, "Ultrashort pulse non-linear optical absorption in transparent media," Opt. Express **13**, 3208-3217 (2005).
36. J. Burghoff, H. Hartung, S. Nolte, and A. Tünnermann, "Structural properties of femtosecond laser-induced modifications in $LiNbO_3$," Appl. Phys. A **86**, 165-170 (2007).
37. H. Zhang, S. M. Eaton, and P. R. Herman, "Low-loss Type II waveguide writing in fused silica with single picosecond laser pulses," Opt. Express **14**, 4826-4834 (2006).

#95835 - $15.00 USD Received 6 May 2008; revised 5 Jun 2008; accepted 8 Jun 2008; published 11 Jun 2008

38. R. Osellame, N. Chiodo, V. Maselli, A. Yin, M. Zavelani-Rossi, G. Cerullo, P. Laporta, L. Aiello, S. De Nicola, P. Ferraro, A. Finizio, and G. Pierattini, "Optical properties of waveguides written by a 26 MHz stretched cavity Ti:Sapphire femtosecond oscillator," Opt. Express **13**, 612-620 (2005).
39. R. Bruckner, "Properties and structure of vitreous silica. I," J. Non-Cryst. Solids **5**, 123-175 (1970).
40. V. R. Bhardwaj, P. B. Corkum, D. M. Rayner, C. Hnatovsky, E. Simova, and R. S. Taylor, "Stress in femtosecond-laser-written waveguides in fused silica," Opt. Lett. **29**, 1312-1314 (2004).

1. Introduction

The advent of high-repetition rate femtosecond lasers is opening new avenues for manipulating thermal relaxation effects [1-4] that control the properties of optical waveguides formed when the ultrashort pulse lasers are focused inside glasses. At low to moderate repetition rates (1-200 kHz), an increase in laser pulse energy leads to formation of larger modification structures as thermal diffusion extends the laser-heated region far outside the focal volume [5, 6]. In this way, isotropic thermal diffusion can compensate for an asymmetric focal heating volume to produce a cylindrically symmetric waveguide cross section [5]. As repetition rate increases, the time between laser pulses becomes shorter than the time for the absorbed laser radiation to diffuse out of the focal volume and heat builds up around the focal volume. This effect was first exploited in the surface micromachining of glass to form smooth, crack-free holes due to laser interaction with a thin sheath of ductile pre-heated glass [7]. Schaffer *et al.* reported a dramatic increase in the size of laser-modified structures formed in the bulk of glass under strong heat accumulation effects with a 25-MHz laser oscillator over structures formed by diffusion-only processes [1]. The combination of high repetition rate and heat accumulation offers fast writing speeds and cylindrically symmetric waveguides together with benefits of annealing and decreased thermal cycling that are associated with low propagation and coupling loss to standard optical fiber [2, 4, 8]. While thermal diffusion and heat accumulation are seen to play similar roles in extending the laser modification volume, the relative contribution of each effect in waveguide formation and the transition between these two phenomena have not been studied experimentally nor addressed in thermal models, particularly in the transition zone from 200-kHz to >1-MHz repetition rate.

In this work, a variable repetition rate femtosecond laser is applied for the first time to uncover the relative contributions of thermal diffusion and heat accumulation in forming optical waveguides. A simple finite-difference thermal diffusion model, previously only applied to 1 MHz repetition rate [4], is now extended to globally predict the heat-modified zone diameter in borosilicate glass (Corning EAGLE2000) for widely varying exposure conditions. By accounting for different laser absorption rates, we find a very good match between experimental and theoretical data in defining the relative contributions of thermal diffusion and heat accumulation at each exposure condition. We can conclusively identify the onset of heat accumulation effects for repetition rates above 200 kHz. We further demonstrate that this heat accumulation transition is significantly shaped by the laser pulse energy and scan speed whose values are also shown to have significant bearing on the quality of the laser-formed optical waveguides. The onset of heat accumulation is therefore not simply defined by the repetition rate, but can be driven by increased pulse energy, reduced scan speed, and commensurate changes in the laser absorption.

In contrast with our previous study of Schott AF45 borosilicate glass [4], a rigorous optimization revealed a common optimum processing zone of 200-mW average power and 10- to 25-mm/s scan speed for writing low-loss waveguides at all repetition rates (0.2 to 2 MHz). Here, strong thermal diffusion from high pulse energy at low repetition rate balances the decreased pulse energy and increased heat accumulation at high repetition rates to produce waveguides with similar dimensions, refractive index profile and propagation loss. These waveguide properties are shown to be independent of laser polarization and pulse durations over a range of 300 to 700 fs. These results are presented in the context of generating waveguides with low insertion loss coupling with single-mode fiber (SMF) and of low-aberration focusing [9] for writing in large depth ranges in the glass. Finally, we report a high temperature stability for waveguides written in the optimum processing window, while

#95835 - $15.00 USD Received 6 May 2008; revised 5 Jun 2008; accepted 8 Jun 2008; published 11 Jun 2008

waveguides written with lower exposure were more lossy and had less stable outer cladding when thermally annealed.

2. Laser writing of waveguides

An amplified fiber laser (IMRA America μJewel D-400-VR) provided ~300-fs pulses (Lorentzian FWHM) at 1045-nm wavelength with repetition rate variable from 200 kHz to 5 MHz and average power of ~500 mW. The collimated beam was a nearly cylindrically symmetric Gaussian with $M^2 = 1.3$ and diameters of ~6×5 mm^2 ($1/e^2$) as measured by a large-area CCD camera (Ophir BeamStar FX 66). The beam slightly overfilled the 5-mm clear aperture of the focusing lenses resulting in ~400-mW average power at target. The laser beam was focused below the surface of a borosilicate glass (Corning EAGLE2000) samples (25×50×1 mm^3). Corning EAGLE2000 glass has similar properties compared with other common borosilicate glasses and was selected for this study due to its wide industrial use in flat panel displays. Aspheric focusing lenses (New Focus 5720) with numerical apertures of 0.25, 0.4 and 0.55 yielded spot sizes ($1/e^2$ diameter) of approximately 3.4, 2.2, and 1.6 μm, respectively. Samples were translated transversely relative to the incident laser at speeds of 2 mm/s to the hardware limit of 100 mm/s using precise air-bearing motion stages (Aerotech ABL1000). The laser power was varied using a half waveplate on a computer-controlled rotation stage before a Glan-laser polarizer to ensure linear polarization at the target, either parallel or perpendicular to the sample motion. To rotate the linear polarization or provide circular polarization, a half or quarter waveplate was inserted after the power attenuator, respectively. The average power and pulse duration were measured with a thermal power meter (Ophir 10A) and an autocorrelator (APE PulseCheck), respectively.

After waveguide inscription, the end facets of samples were ground and polished. The waveguide mode profile, insertion loss and propagation loss were characterized with a 1550-nm laser (Photonetics Tunics-BT) source, fed by Corning SMF28e optical fiber for butt-coupling to the input waveguide facet. The insertion loss was obtained from the power transmitted (Newport 818-IG detector) through the waveguide between two butt-coupling SMF fibers at the input and the output waveguide facet, and normalized to the power propagated by directly butt-coupled input and output fibers. Index matching fluid was applied at the end facets to avoid Fresnel reflection losses and improve measurement accuracy. Mode profiles were obtained by imaging the near-field intensity at the output facet of the waveguide sample with a 60× microscope objective and a phosphor-coated CCD camera (Spiricon SCOR20-1550). Manual translation stages with 100-nm resolution were used to align input/output fibers (Luminos I3000 3-axis) and waveguide samples (Luminos I5000 5-axis).

A commercial refracted near field (RNF) instrument (Rinck Elektronik) provided cross-sectional refractive index profiles with an index resolution of ~10^{-5} and spatial resolution of ~0.5-μm at 633-nm wavelength. To assess thermal stability, samples were annealed at various temperatures up to 900°C in a tube furnace (Sigma-Aldrich Thermolyne 21100) and tested for degraded waveguide properties. Qualitative overhead and cross-sectional images of waveguides were obtained with a white-light Olympus microscope in transmission mode.

3. Heat accumulation versus thermal diffusion effects

3.1 Heat diffusion and accumulation model

To calculate the size of thermally-induced modification zones over a broad range of laser exposure conditions requires knowledge of the temperature distribution as a function of time. We follow a simple radially symmetric thermal diffusion model applied previously by our group in the similar type of borosilicate glass (Schott AF45) [4]. The model assumes spherical Gaussian heat dissipation, so that temperature is calculated as a function of radial position (i.e. $T(r,t)$). The model is therefore valid only for times after heat diffusion has expanded an asymmetric laser-heating focal volume (~1.6-μm transverse spot size × ~4.4-μm depth of focus for NA = 0.55) to a nearly spherically temperature distribution, a condition that is valid for most of the exposure conditions examined here. The model also assumes a static laser

#95835 - $15.00 USD Received 6 May 2008; revised 5 Jun 2008; accepted 8 Jun 2008; published 11 Jun 2008

exposure, and an effective number of laser exposure pulses, $N = 2w_0R/v$, was therefore inferred from scan speed, v, repetition rate, R, and spot size, $2w_0$, that considers the number of laser pulses delivered per spot diameter. This static exposure assumption was validated by the observation of identical modification diameters for static and scanned exposures formed with the same net fluence. Thermal properties for EAGLE2000 were averaged over a temperature range of 23 to 600°C from published data [10].

Radiative transport can be neglected [11] for the small size (tens of microns) of the laser-heated volume in the present work, and as evidenced by a transient thermal lensing study of laser-heated borosilicate glass for high temperatures (~1000°C) [12]. Carr *et al.* [11] noted that shock is a large heat transport factor in laser-heated fused silica, but only in short time frames of ~10 ns and short-distance ranges that can be neglected here where thermal diffusion dominates over the long >500-ns time interval between laser heating pulses.

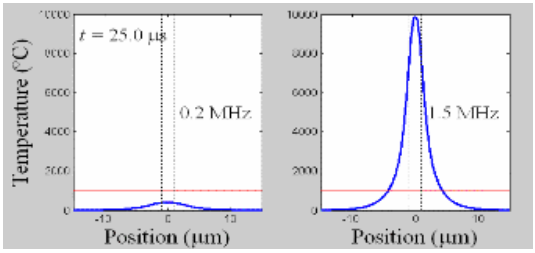

Fig. 1. (3.3 MB) Simulated temperature profile evolution (0 to 25 µs) for static laser exposures (200-nJ absorbed energy/pulse) in Corning EAGLE2000 borosilicate glass for repetition rates of 200 kHz (left) and 1.5 MHz (right). The horizontal red line at T_s = 985°C is the softening point for EAGLE2000 used to define the threshold radius for melting.

Figure 1 shows the temporal evolution of the temperature profile obtained from the thermal model for repetition rates of 0.2 and 1.5 MHz for static laser exposures in EAGLE2000 glass. In both cases, the absorbed pulse energy was 200 nJ and focused by a 0.55-NA lens to match typical waveguide writing conditions. The horizontal line at T_s = 985°C is the softening point for EAGLE2000 and is used to define the threshold radius for melting. At 1.5-MHz repetition rate, the strong laser-induced temperature rise within the ~1.6-µm laser spot builds on top of a slowly building Gaussian heat distribution, yielding a melted volume which expands as further laser pulses are absorbed. At 200-kHz repetition rate, where there is a 7.5-fold greater time between pulses (5 µs), significant diffusive cooling occurs between pulses, resulting in insignificant cumulative heating. At this repetition rate, single-pulse thermal diffusion acts alone in determining the waveguide diameter, which is significantly smaller than that predicted for the 1.5-MHz case. However, we show in the next section that increased laser pulse energy at 200-kHz repetition rate will first increase the diffusion scale length, and then drive heat accumulation to produce a similar melt diameter as for the 1.5-MHz repetition rate case.

3.2 Waveguide diameters

To compare experimental and theoretically calculated diameters, the temperature profile $T(r,t)$ was first calculated for exposure criteria given by the absorbed energy (defining E_0), scan speed (defining number of pulses/spot, N) and repetition rate R (defining frequency of heat source). Solving for the maximum radius, r_{max}, within the last heat cycle where $T(r_{max},t) = T_s$ = 985°C (as in Fig. 1), was interpreted as the modification melt radius defining the radius of the heat-modified waveguide. This radius encapsulates the low-index cladding of the waveguide while the high temperature cycling (Fig. 1) within the laser spot size is expected to define the waveguide core, the region with the highest refractive index change and responsible for light guiding as discussed in Section 3.4. For the present thermal analysis, we therefore follow the cladding diameter. In this paper, we use the term waveguide to describe the overall laser-induced modification zone. Because of similarity with the optical fiber

#95835 - $15.00 USD Received 6 May 2008; revised 5 Jun 2008; accepted 8 Jun 2008; published 11 Jun 2008

geometry, we define the outer heat-modified region with relatively low-index change as the cladding zone, despite the fact that the claddings formed in the laser-written structures do not exhibit discrete cladding modes found in optical fibers. In the model, there were no adjustable parameters. The objective was to study the effects of scan speed, repetition rate and pulse energy and apply the thermal model against the observed waveguide morphologies.

Laser-induced absorption was inferred from the power transmitted through the glass sample. An optical power meter (Ophir 10A) was placed just below the translating sample, so that the entire divergent beam was captured. After accounting for Fresnel reflections at the air-glass interfaces, the transmitted power was converted to a fractional absorption. Experimentally measured absorption values represent an upper bound, as the power meter placed beneath the sample could not detect light reflected by the laser-induced plasma. However, others have shown that only a small fraction (~3%) of light is reflected by the electron plasma under similar laser exposure conditions [19], thus validating the experimentally measured absorption values reported here. Figure 2(a) shows the fractional absorption measured as a function of repetition rate (R = 0.2, 0.5 and 1.5 MHz) for incident pulse energies of 100, 200 and 250 nJ. Previously, we noted only a constant absorption rate of ~50% in Schott AF45 borosilicate glass, where pulse energy (520 nJ) and repetition rate (1 MHz) was not varied in the modeling [4]. The absorption values are shown for 15-mm/s scan speed, and were constant within experiment uncertainty (± 2%) for speeds of 2 to 80 mm/s, consistent with findings in a previous study on Schott D263 borosilicate glass [13]. The absorption increases strongly with pulse energy due to an increased photoionization rate [14], until saturating as evident near 250 nJ. Figure 2(a) demonstrates preliminary evidence of heat accumulation effects, where for constant pulse energy, the absorption increases with repetition rate. As noted for the high 1.5-MHz repetition rate in Fig. 1, incomplete cooling between pulses presents a higher temperature glass to subsequent pulses, which then interact with thermally excited plasma to seed strong avalanche ionization [13].

The diameter of waveguides measured transversely from overhead transmission mode white-light microscopy is shown in Fig. 2(b) as a function of scan speed for incident laser pulse energies of 100, 200 and 250 nJ and 1.5-MHz repetition rate. Heat accumulation effects are clearly evidenced by the strongly increasing diameters with decreasing scan speed. Such a velocity trend would not be observed amongst pulses of the same energy if only thermal diffusion was present. Increased absorbed (incident) laser energy from 40 to 200 nJ (100 to 250 nJ) resulted in significantly higher initial temperatures and more pronounced heat accumulation effects, leading to ~4-fold larger waveguide diameters for this increase in absorbed energy, as shown in Fig. 2(b). However, below an energy (fluence) of 75 nJ (3.8 J/cm^2), there was no evidence of thermal diffusion or heat accumulation effects for all scan speeds tested, as the resulting waveguide diameter did not extend beyond the ~2-µm (horizontal line in Fig. 2(b)) diameter of the laser spot size.

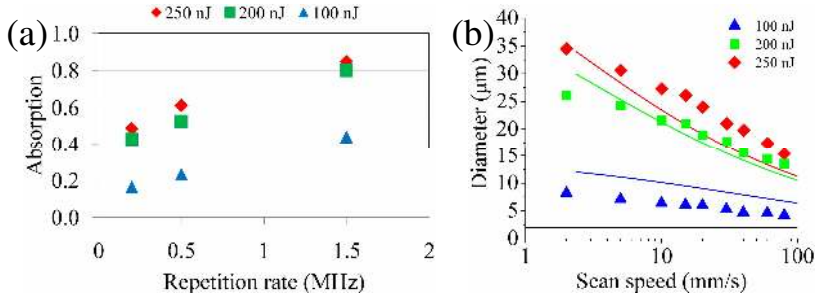

Fig. 2. Absorption (a) versus repetition rate for pulse energies of 100, 200 and 250 nJ, and transverse waveguide diameter (b) versus scan speed for pulse energies of 100, 200 and 250 nJ at 1.5-MHz repetition rate. Colored curves show calculated diameter. The black line at 2-µm diameter shows the approximate spot diameter ($2w_0$) of the laser.

#95835 - $15.00 USD Received 6 May 2008; revised 5 Jun 2008; accepted 8 Jun 2008; published 11 Jun 2008

The solid lines in Fig. 2(b) are the waveguide diameters predicted by the thermal model, which are seen to closely follow the experimental data within ~10% error at the higher pulse energies. Calculated values for 100-nJ pulse energy overestimate the diameter by ~25%. The assumption of spherical symmetry in the model is breaking down here as heat-modified diameters of ~5 μm or smaller no longer exceed an ellipsoidal-like heating volume of $2w_0$ = 1.6-μm transverse diameter by ~4.4-μm depth of focus, thereby overestimating the temperature. Discrepancy between theory and experiment is also attributed to the uncertain thermal properties of EAGLE2000 glass above 600°C.

To gain insight into the separate roles played out by thermal diffusion and heat accumulation, the transverse modification diameter was examined as the repetition rate was increased at a constant net fluence exposure or dosage, defined as:

$$\mathrm{NF} = \frac{2w_0 R}{v} F_p \tag{1}$$

where w_0, R, and v were previously defined, $F_p = E_p/\pi w_0^2$ is the fluence per pulse, and E_p is the incident laser pulse energy. Equation (1) indicates two approaches for driving uniform fluence exposure as the repetition rate is increased: pulse energy (and fluence per pulse) can be held constant so that scan speed must be increased to maintain a constant ratio of R/v, or laser pulse energy can be reduced to maintain a constant value for RF_p (constant average power).

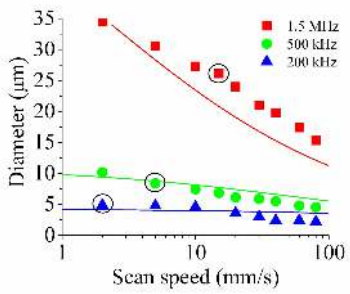

Fig. 3. Waveguide diameters plotted against scan speed for 250-nJ pulse energy and repetition rates of 0.2, 0.5 and 1.5 MHz. The circled data points show melt diameters for NF = 2 kJ/cm^2. Calculated thermal model values of the melt diameter are shown by the solid curves.

The former approach for maintaining constant net fluence is shown in Fig. 3, where the transverse modification diameter is plotted as a function of scan speed for a constant pulse energy of 250 nJ at repetition rates of 0.2, 0.5 and 1.5 MHz. As expected, the transverse waveguide diameter increases with increasing net exposure, through increased repetition rate and increased dwell time (decreasing scan speed). The widely varying diameters in Fig. 3 is attributed to heat accumulation, since the effect of thermal diffusion is held constant for a pulse energy fixed at 250 nJ. The steepening slopes as repetition rate increases are strong evidence of increased heat accumulation. Time-resolved spectroscopic recordings [15] of the laser-induced emissions in EAGLE2000 also provide evidence of heat accumulation effects as short (<100-ns decay time) bursts of spectral emissions at 100-kHz rates give way to nearly continuous broadband emissions (>1-μs decay time) at 2-MHz repetition rate. The open circles in Fig. 3 showing modification diameters of 5, 8 and 26 μm were obtained for identical net fluence exposure of 2 kJ/cm^2, corresponding to identical ratios of R/v = 0.2 MHz / 2 mm/s, 0.5 MHz / 5 mm/s, and 1.5 MHz / 15 mm/s, respectively. The data clearly shows strong heat accumulation effects by the large 5-fold increase in waveguide diameter even when scan speeds are scaled down with increasing repetition rate to deliver uniform fluence exposure. Good agreement (±10%) is observed between theoretical and experimental values of waveguide diameter.

#95835 - $15.00 USD Received 6 May 2008; revised 5 Jun 2008; accepted 8 Jun 2008; published 11 Jun 2008

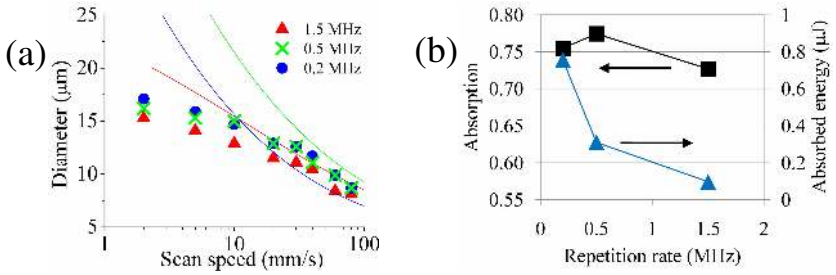

Fig. 4. Transverse waveguide diameter (a) as a function of scan speed for repetition rates of 0.2, 0.5 and 1.5 MHz at a constant average power of 200 mW. Data points are experimental diameters and solid curves are diameters predicted by model; corresponding values of absorption and absorbed energy (b) versus repetition rate at 200-mW average power.

Alternatively, heat-modification diameters formed under constant average power of E_pR = 200 mW are shown in Fig. 4(a) for varying scan speed. Under these conditions, the melt diameters increase with dwell time (decreasing v), as expected, but values otherwise remain nearly constant (within ~15%) at each scan speed where net fluence exposure is the same for each of the 0.2, 0.5 and 1.5 MHz repetition rates. This apparent absence of heat accumulation effect arises from a fortuitous combination of exposure conditions where much higher pulse energy, and therefore stronger thermal diffusion, is now delivered at lower repetition rate. This higher energy drives up absorption (~75%) to match values previously only seen at higher repetition rate as shown in Fig. 4(b). In this way, the 8-fold higher pulse energy at 0.2 MHz drives significantly more laser energy of 0.75 μJ into the glass each pulse in contrast with 0.1 μJ/pulse dissipation at 1.5 MHz, as shown by the right vertical axis data in Fig. 4(b). Much stronger thermal diffusion is now driven at low repetition rate, extending the modification zone dramatically to match that produced by low energy absorption in the strong heat accumulation at high repetition rates. Good agreement between theory and experiment is observed at a repetition rate (pulse energy) of 1.5 MHz (133 nJ), but discrepancies are noted at 500 kHz (400 nJ) and 200 kHz (1 μJ), particularly at scan speeds below 10 mm/s. At these lower repetition rate conditions, the combination of high pulse energy (>400 nJ) and low scan speed (<10 mm/s) resulted in damaged tracks visible by microscope inspection. Moreover, these damage tracks caused high scattering of laser light in the focal volume that led to overestimated absorption values in Fig. 4(b), and therefore calculation of overly large modification diameters for the 200 and 500-kHz data when speeds were less than 10 mm/s.

The combination of thermal events in Fig. 4 is somewhat unique at the present 200-mW power level in balancing structure diameter that we show in Section 4 to provide the lowest insertion-loss waveguides for coupling to SMF. This balancing of waveguide diameter at constant net fluence [Eq. (1)] is not available by velocity tuning (constant R/v data points in Fig. 3) which always increases waveguide diameter as repetition rate increases.

3.3 Heat accumulation threshold

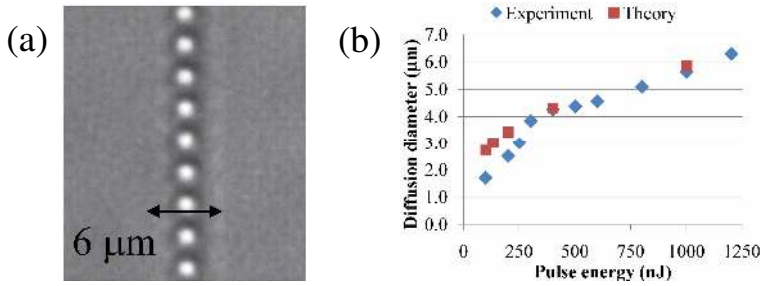

Fig. 5. Overhead microscope image (a) showing diffusion zones from single pulses with 1-μJ pulse energy. Experimental and calculated modification diameters (b) from single-pulse diffusion versus incident pulse energy.

#95835 - $15.00 USD Received 6 May 2008; revised 5 Jun 2008; accepted 8 Jun 2008; published 11 Jun 2008

To estimate the onset of heat accumulation effects, it was first necessary to experimentally verify the range of diffusion-only effects for a single pulse exposure. This was achieved by lowering the repetition rate to 40 kHz with an acousto-optic modulator and increasing the scan speed to 100 mm/s such that modification tracks opened up into nearly isolated interaction spots of 2.5-μm spacing as shown in Fig. 5(a). For this example of relatively strong laser interaction at 1-μJ pulse energy, thermal diffusion defines a faint ~6-μm diameter zone that extends 4-fold larger than the ~1.6-μm spot size, also seen as bright circular spots in Fig. 5(a). Figure 5(b) plots the experimental values of diffusion diameter as a function of pulse energy, together with melt diameter predicted by the thermal diffusion model for reaching 985°C in a single laser pulse. There is very good agreement above 4-μm diameter, while theory overestimates values at lower pulse energy as we expect when the spherical diffusion diameter ($2r_{max}$ = 4 μm) is less than the ~4.4-μm depth of focus, as explained above.

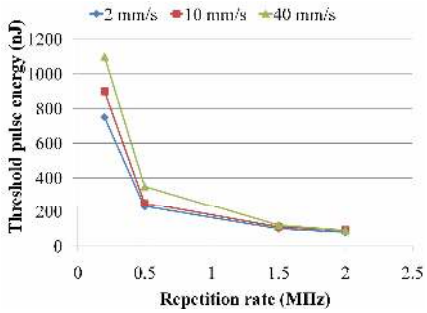

Fig. 6. Experimental values of threshold pulse energy for onset of heat accumulation as a function of laser repetition rate for scan speeds of 2, 10 and 40 mm/s and NA = 0.55 focusing.

We define an onset threshold for heat accumulation as the minimum laser pulse energy required to increase the waveguide diameter 2-fold over the diameter produced by diffusion in a single-pulse interaction as determined in Fig. 5(b). Experimental values for this energy threshold are shown Fig. 6 as a function of repetition rate (200 kHz to 2 MHz) and for various scan speeds (2, 10, and 40 mm/s) and should be compared with a single-pulse damage threshold of 50 nJ (2.5 J/cm^2 fluence) for creating a structure visible under an optical microscope, which was invariant with repetition rate. In contrast, the energy threshold for heat accumulation decreased sharply from values of ~900 nJ at 200 kHz to ~80 nJ at 2 MHz and was only weakly dependent on scan speed, varying from 750 to 1100 nJ at 200 kHz compared with 80 to 90 nJ at 2 MHz for scan speeds of 2 to 40 mm/s. At 200-kHz repetition rate, a stronger source of thermal diffusion provided by higher pulse energy is thus available to initiate cumulative heating to compensate for the lower pulse delivery rate compared with higher repetition rates. In this R = 0.2 to 2 MHz range, the diffusion scale length $\sqrt{D/R}$ decreases from 1.6 to 0.5 μm, indicating that the effective laser heating volume shrinks dramatically with increasing repetition rate, thereby reducing the threshold pulse energy for heat accumulation. For R > 1 MHz, the thermal diffusion scale length of ~0.7 μm falls inside the laser waist radius of w_0 = 0.8 μm, resulting in asymptotic minimum limit of the heat accumulation threshold energy to ~80 nJ at 2-MHz repetition rate in Fig. 6.

Beyond 2 MHz, the available laser pulse energy was below 80 nJ, preventing the observation of heat accumulation effects in the present borosilicate glass. Similarly, when the laser was operated at 100-kHz repetition rate, the 2-μJ maximum pulse energy available was insufficient to drive heat accumulation effects beyond a large thermal diffusion diameter of ~8 μm. Hirao and coworkers inferred a 10-μs cooling time (to <100°C) in borosilicate glass (Corning 0211) when exposed to a single laser pulse of 220-fs duration and 600-nJ energy focused by a 0.4-NA lens [12]. While this suggests a ~100-kHz threshold for heat accumulation, the data in Fig. 6 indicates that this threshold is in fact variable with the repetition rate, and strongly dependent on the laser pulse energy and scan speed, and is also likely dependent on other changes in laser parameters, spot size and material.

#95835 - $15.00 USD Received 6 May 2008; revised 5 Jun 2008; accepted 8 Jun 2008; published 11 Jun 2008

The experimental and well-matched theoretical results presented in Figs. 1-6, conclusively show that both thermal diffusion and heat accumulation play significant roles in defining the waveguide morphology at repetition rates greater than 200 kHz. The threshold pulse energy for driving sufficient thermal diffusion to initiate heat accumulation was observed to decrease with increasing repetition rate, before approaching a minimum modification threshold at ~1 MHz repetition rates when the diffusion scale length falls below the laser's waist radius.

3.4 Cross sectional refractive index profiles

High-resolution refracted-near field (RNF) measurements [16] provided cross-sectional refractive index profiles of waveguides across a wide range of laser exposure conditions. RNF profiles in Fig. 7 present the interesting case in Section 3.2 where waveguides of similar diameter were generated across the 0.2 to 2 MHz range of repetition rates by holding constant the net fluence exposure with a fixed 200-mW power. Here, waveguides were written with a 0.55-NA lens, 150-μm depth, 25-mm/s scan speed and repetition rates of 0.2, 0.5, 1, 1.5, and 2 MHz. As will be shown in Section 4.1, this combination of average power and scan speed also provided optimum waveguides for low-insertion loss at each repetition rate. The core-cladding structure is similar to other waveguides formed with high-repetition rate lasers [4, 17] and is the result of rapid cooling of the melted volume. Insight into the core-cladding structure can be gained from the animation in Fig. 1. The core of the waveguide structure is attributed to the high temperature impacts induced within the ~1.6-μm spot size by each laser pulse while the outer lower-contrast cladding is formed by a more slowly evolving near-Gaussian temperature distribution, with the overall size determined by the largest diameter where the temperature exceeds the melting point. Because of the variable temperature across the modified zone, the cooling rates are highly nonuniform [1], and therefore are expected [18] to lead to a nonuniform distribution of the final glass density (refractive index).

The depth of the small, dark spot near the bottom of the structures in Fig. 7 was observed to be independent of average power (50 to 400 mW), repetition rate (0.2 to 5 MHz), and writing speed (5 to 80 mm/s), except for pulse energies >1 μJ at 200-kHz repetition rate, where the dark spot shifted towards the sample surface by several microns. We attribute this spot to the focal plane location, with the images showing that most of the laser energy was deposited upstream of the focus. With increased pulse energy (not shown), the modified zones expanded upwards towards the surface, but the dark focal spot remained at the same depth, showing no evidence of self focusing, except when pulse energies >1 μJ resulted in peak powers exceeding the critical self-focusing power of ~3 MW at 1045-nm wavelength [19].

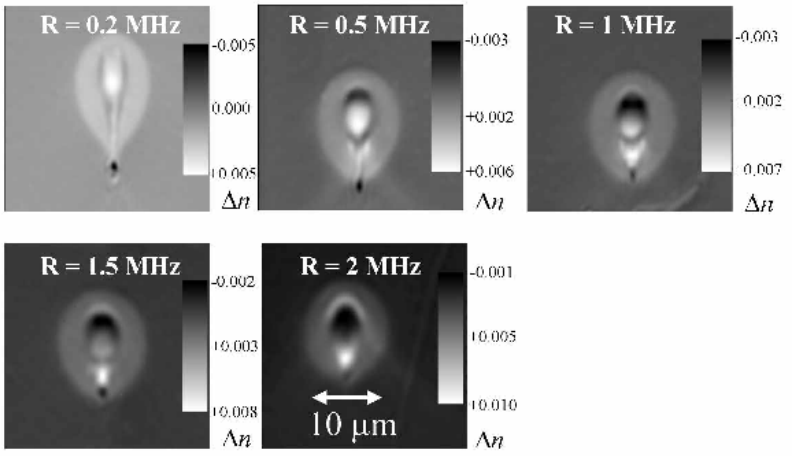

Fig. 7. Cross-sectional refractive index profiles from RNF measurements of waveguides written with 0.55-NA focusing, 200-mW power, 150-μm depth, 25-mm/s scan speed and repetition rates of 0.2, 0.5, 1, 1.5, and 2 MHz. The writing laser was incident from the top.

#95835 - $15.00 USD Received 6 May 2008; revised 5 Jun 2008; accepted 8 Jun 2008; published 11 Jun 2008

At 200-kHz repetition rate, the waveguide has an elliptical-like central core guiding region (elongated white region) with peak Δn = +0.005 in a 3.4×6.9-μm^2 area, and an outer elliptical-like heat-modified cladding of peak Δn = +0.001 in a 11.1×18.0-μm^2 area that is defined by diffusion from an asymmetric focal volume. The waveguide is elliptical (~1.6:1 aspect ratio) due to thermal diffusion from a laser heating volume extended vertically by self focusing effects as well as by minimal heat accumulation at this repetition rate. A progression towards more narrow and elongated structures is expected as the repetition rate is further reduced, approaching the cross section typically observed in 1-kHz repetition rate fabrication [20].

At 500-kHz repetition rate, owing to increased heat accumulation, a more circular guiding and cladding cross section are observed with a central core of peak Δn = +0.006 in a ~3.7×5.4-μm^2 area that forms an optical guide. Also noted is a new small region of positive refractive index change formed immediately below the main guiding region. At 1-MHz repetition rate, this region below the core has increased in size and magnitude to a peak Δn = +0.007 in a ~2.2×3.1-μm^2 area. This region is now responsible for waveguiding of 1550-nm light but the mode also extends into the weaker central core (peak Δn = +0.005) to yield two transverse modes when formed with a higher average power exposure (> 250 mW).

At 1.5-MHz repetition rate, the guiding region has clearly transitioned to below the central core to form a small and slightly elliptical region (~2.1×3.1-μm^2 area) of peak Δn = +0.008. Interestingly, the central region is no longer guiding, and dominated by a large volume of negative refractive index of Δn ~-0.002. Despite the ellipticity, the mode profile at 1550 nm is circular, as described below. At 2-MHz repetition rate, the guiding region has a peak Δn = +0.010. Above this repetition rate, the pulse energy dropped below the heat accumulation threshold of ~90 nJ (Fig. 6) to form sufficiently strong guiding structures.

For repetition rates of 0.2 to 2 MHz, the transverse cladding diameter was nearly constant at ~11 μm, consistent with Fig. 4, where diameters were measured from overhead by white-light microscopy. The peak refractive index change in the guiding region increased from 0.005 to 0.010 with 0.2 to 2 MHz increase in repetition rate. The vertical distance between the focal plane (small dark spot) and the center of the waveguides decreased from ~12 μm at 200-kHz repetition rate to ~3 μm at 2-MHz repetition rate, which is attributed to the decreased peak intensity resulting in preferential absorption closer to the focus location. The depth of the guiding core structure was also found to follow a similar trend, with the vertical offset varying from ~13 μm at 200 kHz to ~2 μm at 2 MHz. Although evidence of self focusing was not supported by the observation of a constant focus plane depth in these structures, it is possible that weak self focusing and plasma defocusing may contribute to the variation in refractive index zone morphology with repetition rate.

To quantitatively model the complex structures found in the refractive index profiles as shown in Fig. 7, one requires experimental verification of evolving temperature profiles [21] that our group is presently studying with time-resolved and imaging spectroscopy [15] as well as accurate models of glass density changes for the differing cooling rates [22]. Other sources of refractive index modification such as shockwave propagation also lead to formation of rarefied cores surrounded by dense shells [23, 24], features that also appear to contribute to the refractive index changes seen in Fig. 7.

4. Waveguide processing window

The properties of femtosecond laser written waveguides in bulk glass depend strongly on laser exposure conditions such as repetition rate [3], scan speed, average power, wavelength [25], pulse duration [20, 26-28], polarization [26, 29], numerical aperture, and focus depth [30, 31]. The first three parameters were found to play the strongest role in controlling waveguide properties in EAGLE2000, and are discussed in Section 4.1. Section 4.2 presents the effects of pulse duration and polarization on waveguide properties while Section 4.3 discusses the role of numerical aperture on spherical aberration for fabricating deep waveguides for 3-D

#95835 - $15.00 USD Received 6 May 2008; revised 5 Jun 2008; accepted 8 Jun 2008; published 11 Jun 2008

applications. Waveguides can also be formed in EAGLE2000 with frequency doubled 522-nm light, but without any significant advantage over the present 1045-nm results.

4.1 Repetition rate, scan speed and average power

Figure 8 summarizes waveguide properties as a function of average laser power and scan speed for 1.5-MHz repetition rate and NA = 0.55 focusing at 150-µm depth. Insertion loss (IL) has been classified by red, blue, and black squares representing low (<3 dB), medium (3 to 6 dB) and high (>6 dB) insertion loss, respectively. Waveguides exhibiting multiple transverse modes and typically damaged morphology, written with the highest laser exposures (high power and dwell time) are found at the top-left corner (black diamond data points) of the graph. Conversely, the bottom-right corner indicates underexposed waveguides where the index change was too low to efficiently guide 1550-nm light. At 1.5-MHz repetition rate, the lowest insertion losses for fiber-waveguide-fiber coupling (IL = 1.2 dB; 2.5-cm long waveguide) were observed over a large 10-25 mm/s range of scan speeds but in a narrow 200 ± 10 mW average power range (encircled data in Fig. 8).

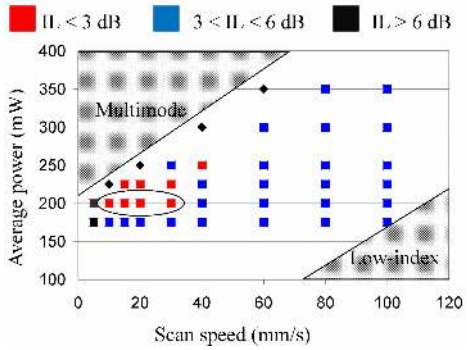

Fig. 8. Processing window map: waveguide properties as a function of average power and scan speed for 1.5-MHz repetition rate.

Similar analysis was carried out for waveguides formed with 0.2, 0.5, 1 and 2-MHz repetition rates and in all cases, revealed a surprisingly similar processing window of 200 mW power and 10 to 25 mm/s scan speed for lowest insertion loss waveguiding. The minimum insertion loss at each repetition rate is presented in Fig. 9(a). Over the wide repetition rate range, the generated waveguides had similar shape (~2.5 µm core and 11 µm cladding diameters) but generated a small increase in refractive index contrast of 0.005 to 0.01 as shown in Fig. 7 that is responsible for the decrease in the waveguide mode-field diameter (MFD) also plotted in Fig. 9(a). The mode field diameters are an average of Gaussian fit diameters ($1/e^2$ of intensity) along *x* and *y* axes and have a greater than 90% correlation for all modes measured. This 200-mW exposure window appears consistent with the optimum 250-mW power found by Osellame *et al.* for generating low-loss waveguides in phosphate glass at repetition rates of 505 to 885 kHz [3].

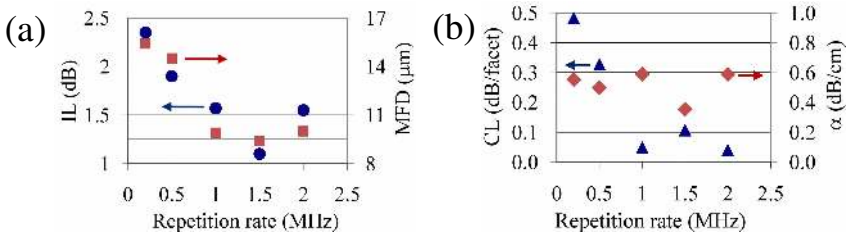

Fig. 9. Measured insertion loss and mode field diameter (a) and coupling and propagation loss (b) versus repetition rate for waveguides written with 200-mW average power and 15-mm/s scan speed. Waveguides were formed 150 µm below the surface with a 0.55-NA lens.

#95835 - $15.00 USD Received 6 May 2008; revised 5 Jun 2008; accepted 8 Jun 2008; published 11 Jun 2008

The decreasing IL with increasing repetition rate in Fig. 9(a) is associated with increasingly stronger heat accumulation effects beginning at ~0.2 MHz that result in stronger refractive index change and smaller MFD for best coupling to optical fibers at 1.5 MHz. The increased insertion loss from 1.5 to 2 MHz is attributed to inadequate laser pulse energy (100 nJ) at 2 MHz for driving sufficient laser heating above the ~90-nJ threshold for heat accumulation. Beyond 2-MHz repetition rate, only narrow ~2-μm diameter waveguides were formed that were barely guiding and showed no evidence of heat accumulation effect.

A large part of the insertion-loss variation in Fig. 9(a) follows from the variation of MFD, also plotted in the same graph, which leads to large coupling loss with optical fiber when the waveguide MFD does not match the 10.5-μm MFD of the fiber (1550-nm wavelength). The expected facet coupling loss (CL) values shown in Fig. 9(b) were estimated using an overlap integral [32] between the measured waveguide mode profile and a Gaussian representation of the fiber mode (10.5-μm diameter), yielding a minimum coupling loss of < 0.1 dB/facet in the 1-2 MHz range. Removing this facet coupling loss from the insertion losses in Fig. 9(a) provides an estimate of the waveguide propagation losses, α, (Fig. 9(b)) which is somewhat constant with repetition rate but reaches a minimum of ~0.35 dB/cm at 1.5-MHz repetition rate, where fiber coupling and heat accumulation are both the most efficient.

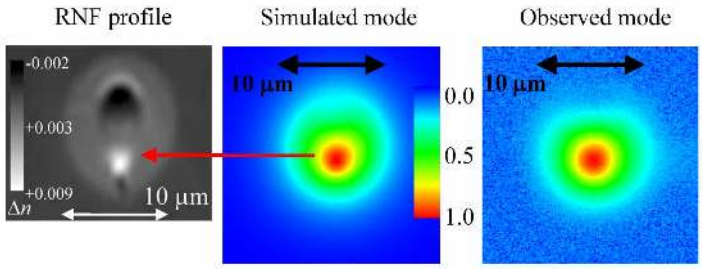

Fig. 10. Waveguide fabricated with 1.5-MHz repetition rate, 200-mW power, 0.55-NA lens, 150-μm depth and 15-mm/s scan speed: refractive index profile, simulated mode and measured mode. Red arrow indicates position of mode relative to waveguide cross section.

The refractive index profile for the optimum waveguide at 15-mm/s scan speed (1.2-dB insertion loss, ~0.3-dB/cm propagation loss) is shown in Fig. 10. The refractive index profile was imported into a numerical mode solving routine (Lumerical MODE Solutions 2.0) to generate the simulated mode profile for 1550-nm light, aligned over the positive index (white spot) guiding region as shown by the red arrow. The simulated profile accurately predicts the experimentally measured mode profile, confirming the accuracy of the RNF measurements.

4.2 Pulse duration and polarization

In contrast to waveguides written in fused silica, where polarization was found to strongly affect the waveguide properties [26, 29], no detectable difference in insertion loss or mode size was found when waveguides were formed with linear (electric field vector parallel or perpendicular to scan direction) or circular polarization in EAGLE2000 borosilicate glass. The laser pulse duration was varied from ~300 to 700 fs (Lorentzian FWHM) by translating a prism in the compressor. In EAGLE2000, waveguide properties were invariant to pulse duration over this range. This also contrasts recent results in fused silica, where pulse duration was observed to strongly affect waveguide mode size and loss [26].

The sensitivity to pulse duration and polarization in fused silica is associated with form birefringence arising from nanogratings formed within the laser-modified volume [33]. In borosilicate glass, nanogratings have not been observed [34], and such polarization and pulse-duration dependence may possibly be erased by the strong thermal annealing [34] effects expected at the high MHz repetition rates applied here to EAGLE2000.

Due to energy depletion, self focusing and plasma defocusing, pulse duration strongly influences the spatial distribution of the energy density in the focal volume [35, 36]. At 1-kHz repetition rate, where heat accumulation is not present, the dependence of waveguide

#95835 - $15.00 USD Received 6 May 2008; revised 5 Jun 2008; accepted 8 Jun 2008; published 11 Jun 2008

properties on pulse duration in lithium niobate [36] and fused silica glass [37] was attributed to nonlinear pulse propagation. However, in the heat accumulation regime, nearly spherically-symmetric thermal diffusion washes out the elliptical distribution of energy in the focal volume to yield waveguides with cross sections that are relatively circular, as seen in Fig. 10, where a waveguide aspect ratio of ~1.3:1 is significantly more symmetric than the ~2.8:1 aspect ratio of the focal volume. Therefore, one would expect pulse duration, despite its affect on the energy distribution at the focus, to play a lesser role on the properties of waveguides fabricated in the heat accumulation regime.

4.3 Spherical aberration

To take advantage of femtosecond laser writing of waveguides in all three dimensions, one must carefully address the spherical aberration at the air-glass interface, which varies dramatically with the focusing depth [30, 31]. Improvements are found with oil-immersion lenses [2, 3, 19], collars for variable depth correction [9] and asymmetric focusing with rectangular beam apertures [31]. In the present paper, we examine for the first time the combination of strong heat accumulation effects to drive spherically symmetric heat flow, and compensate for an axially elongated focal volume as we attempt to decrease the numerical aperture (NA < 0.55) of our focusing lens and reduce the spherical aberration effect. The objective is to extend the practical working distance for writing similar-quality waveguides.

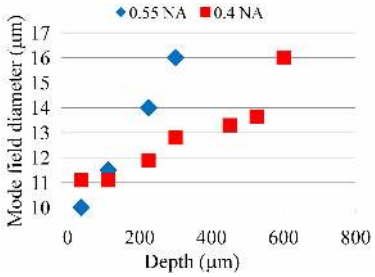

Fig. 11. Mode field diameter versus focusing depth for waveguides formed with 1.5-MHz repetition rate, 15-mm/s scan speed with 0.55 NA (230 mW) and 0.4 NA (200 mW).

For the cumulative heating regime of 0.55-NA focusing applied in the previous sections (200 mW, 1.5 MHz, 15 mm/s) for optimal waveguide writing, waveguides with similar low loss and mode size could only be obtained in a narrow depth range of d = 50 to 200 μm. Figure 11 shows the MFD of these waveguides to increase 60% from 10 μm at 50-μm depth to 16 μm at 300-μm depth, spherical aberration precluding a deeper waveguide writing range. Much deeper waveguide writing was possible with the 0.25-NA lens, but 5-fold lower peak intensity at the maximum available laser power (400 mW) yielded only small diameter waveguides and weak refractive index change. A better balance was found with the 0.4 NA lens, providing only a small increase in MFD from ~11.0 to 13.5 μm as the depth was increased from d = 50 to 520 μm. The measured propagation loss of ~0.35 dB/cm was nearly independent of focal depth. In comparison to 0.55-NA focusing, a 15% higher average power of 230 mW was necessary to partially compensate for the ~38% larger spot size.

The ability to write waveguides to depths of 520 μm is a substantial improvement over the maximum depth of ~200 μm reported by other groups employing MHz repetition rate femtosecond lasers with higher NA focusing objectives [2, 38]. Further increase in this depth range is anticipated for intermediate focusing condition between 0.25 and 0.4 NA and by applying higher power femtosecond laser systems to compensate for the larger focal spot size.

5. Thermal stability of waveguides

For the first time, we report the thermal stability of femtosecond-laser written waveguides formed in the cumulative heating regime. Waveguides were written at 230-mW power, 1.5-MHz repetition rate, 0.4-NA, 150-μm depth and 8-20-mm/s scan speed. After waveguide

#95835 - $15.00 USD Received 6 May 2008; revised 5 Jun 2008; accepted 8 Jun 2008; published 11 Jun 2008

characterization, the EAGLE2000 sample was baked for 1 hour in a tube furnace in repeated heating and testing cycles of increased temperature in 100°C steps. A peak temperature of 800°C was tested that exceeds the annealing point of 722°C, the temperature at which stresses are relieved after several minutes, but remains below the softening point of 985°C at which the glass deforms under its own weight. For reference, the strain point of 666°C is the temperature below which glass can be rapidly cooled without introducing stresses.

Figure 12 shows the mode profile (a) and overhead morphology (b) of the waveguide written with intermediate 15-mm/s scan speed for increasing annealing temperature. There is little change in the mode size and waveguide morphology at temperatures up to 500°C. At 600°C, the mode diameter increased ~10% and there is less contrast in cladding. At 700°C, the mode diameter increased ~40% compared with the unheated sample (25°C), and the cladding is barely visible. At the last heating step of 800°C, the mode was undetectable due to high losses and the cladding has completely disappeared.

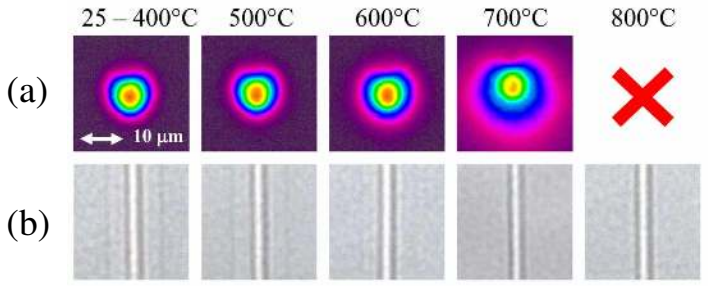

Fig. 12. The 1550-nm mode profile (a) and overhead microscope image (b) at increasing annealing temperatures for waveguides fabricated with 240-mW power, 1.5-MHz repetition rate, 0.4 NA, 150-μm depth and 15-mm/s scan speed. The size scale applies to all images

Figure 13 shows the annealing trends for the mode field diameter (a) and insertion loss (b) for scan speeds of 8 to 25 mm/s. Above 500°C, the MFD and IL for all waveguides tested increased with temperature, with the degree of degradation being smallest for the waveguides written with the lowest speed or highest net fluence. Glass has a frozen-in structure that depends on the cooling rate which corresponds to a fictive temperature of the equilibrium melt [39]. Waveguides fabricated with the highest net fluence are expected to cool fastest from the highest temperatures, creating modification structures with the highest fictive temperatures. Therefore, waveguides written at the highest exposure required annealing at higher temperatures to undo the thermal history of the laser-modified glass and restore its properties to that of the unmodified bulk. Further, the disappearance of the cladding before the central core in Fig. 12 is attributed to a lower fictive temperature in the outer cladding.

For the waveguide written with the minimum laser exposure (20 mm/s), the 600°C anneal step increased the MFD and IL by 10% and 3.5 dB, respectively, and the waveguide mode became undetectable after the 700°C step. In contrast, the maximum net exposure waveguide (8 mm/s) survived all annealing steps, accumulating only a small 5% and 0.7 dB increase, respectively, in MFD and IL across all annealing steps to 800°C.

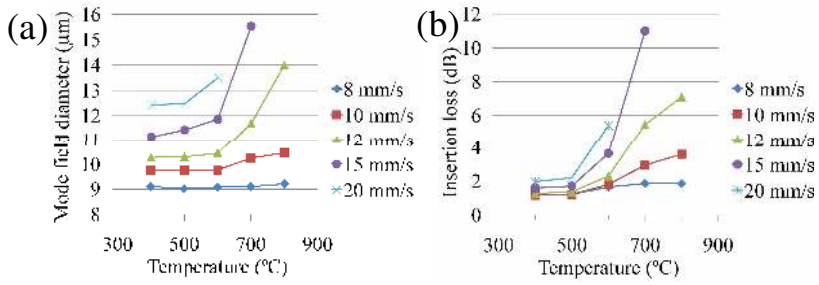

Fig. 13. Mode field diameter (a) and insertion loss (b) versus one-hour baking cycles at indicated temperature (same waveguide exposure conditions as Fig. 12)

#95835 - $15.00 USD Received 6 May 2008; revised 5 Jun 2008; accepted 8 Jun 2008; published 11 Jun 2008

By heating the sample above the annealing point (722°C) and then slowly cooling it, the radial stress that may be developed during waveguide formation is relaxed [40]. For waveguides written at slow speeds of 8 and 10 mm/s, the mode field diameter and insertion loss show strong resistance to heating at 800°C. This indicates that stress-optic contribution to the refractive index modification is small. Thermal annealing did not improve waveguide losses, which others have reported in fused silica and attributed to stress relaxation [40] and reduction of waveguide roughness and refractive index fluctuations [28]. The propagation loss follows a similar trend as the insertion loss in Fig. 13(b), varying from 0.3 to 0.6 dB/cm from 400 to 800°C for the strongest waveguide written at 8 mm/s, and from 0.7 to 1.8 dB/cm from 400 to 600°C for the weakest waveguide written at 20 mm/s.

Waveguides written in EAGLE2000 glass with 1-kHz repetition rate were much less stable than the present 1.5 MHz results, undergoing an 80% increase in MFD after annealing at 500°C, and resulting in undetectable guiding at 1550 nm after annealing at 750°C [20]. We attribute the higher temperature stability of waveguides written with 1.5-MHz repetition rate to the higher fictive temperatures driven by the cumulative heating regime.

6. Summary

In summary, we applied a variable repetition rate femtosecond laser to elucidate the smooth transition from single-pulse thermal diffusion at low repetition rate (<200 kHz) to heat accumulation-dominated modification at high repetition rates (>1 MHz). At 200-kHz repetition rate, a strong source of thermal diffusion provided by ~900-nJ pulse energy was required to initiate heat accumulation, while at 2-MHz repetition rate, where pulses are delivered at 10-fold faster rates, a much lower energy of ~80-nJ was sufficient to drive heat buildup. By accounting for the variable absorption with incident pulse energy and repetition rate, a simple thermal diffusion model provided accurate predictions of experimentally measured waveguide diameters for a wide range of scan speed, pulse energy and repetition rate. A novel laser processing window was presented for writing low-loss waveguides across the large 0.2 to 2.0 MHz range of repetition rates tested here. By holding laser power constant and delivering the same net fluence exposure at each repetition rate, strong thermal diffusion from high energy pulses at 200-kHz repetition rate compensated for strong heat accumulation effects with low pulse energy delivered at high repetition rate to produce waveguides of similar diameter and strong guiding at 1550 nm wavelength. Overall, waveguides formed with the strongest heat accumulation effects (1.5 MHz) provided the minimum propagation loss of ~0.3 dB/cm and best mode coupling to standard telecom fiber. Such waveguides were shown to be very stable to temperatures of up to 800°C that is highly attractive for optical sensing applications in high temperature environments. We also exploited the spherical symmetry of strong heat accumulation effects to compensate for asymmetric laser heating volumes caused by spherical aberration and low-NA lenses to enable waveguide formation over large depths up to 520 μm below the surface. This combination of results provides much improved flexibility and control for generating optical circuits in all three dimensions in borosilicate glasses for promising new applications in optical communication, biomedical, and sensing industries.

Acknowledgments

We thank Sergey Reznik for technical support, Andrew Yick for MATLAB animation, Ethan Klem for assistance with thermal annealing, and Prof. Stefan Nolte, Dr. Jonas Burghoff and Tariq Rafique for helpful discussions. We thank Stefan Rinck from Rinck Elektronik for RNF characterization. This work was supported by funding from the Canadian Institute for Photonics Innovation and the Natural Sciences and Engineering Research Council of Canada.

#95835 - $15.00 USD Received 6 May 2008; revised 5 Jun 2008; accepted 8 Jun 2008; published 11 Jun 2008